Journal of Dispersion Science and Technology

ISSN: 0193-2691 (Print) 1532-2351 (Online) Journal homepage: https://www.tandfonline.com/loi/ldis20

Apparatus-dependent sol-gel synthesis of TiO_2 nanoparticles for dye-sensitized solar cells

Jyoti Bansal, Sanjay Kumar Swami, Akanksha Singh, Tarnija Sarao, Viresh Dutta, A. K. Hafiz & Shailesh Narain Sharma

To cite this article: Jyoti Bansal, Sanjay Kumar Swami, Akanksha Singh, Tarnija Sarao, Viresh Dutta, A. K. Hafiz & Shailesh Narain Sharma (2019): Apparatus-dependent sol-gel synthesis of TiO_2 nanoparticles for dye-sensitized solar cells, Journal of Dispersion Science and Technology, DOI: 10.1080/01932691.2019.1699427

To link to this article: https://doi.org/10.1080/01932691.2019.1699427

JOURNAL OF DISPERSION SCIENCE AND TECHNOLOGY
https://doi.org/10.1080/01932691.2019.1699427

Apparatus-dependent sol-gel synthesis of TiO_2 nanoparticles for dye-sensitized solar cells

Jyoti Bansal[a,b], Sanjay Kumar Swami[a], Akanksha Singh[a], Tarnija Sarao[c], Viresh Dutta[d], A. K. Hafiz[b], and Shailesh Narain Sharma[a]

[a]CSIR-National Physical Laboratory, New Delhi, India; [b]Centre for Nanoscience and Nanotechnology, Jamia Millia Islamia, New Delhi, India; [c]Department of Physics, Amity University, Noida, Uttar Pradesh, India; [d]Photovoltaic Lab, Centre for Energy Studies, Indian Institute of Technology Delhi, New Delhi, India

ABSTRACT

Synthesis of titanium dioxide nanoparticles (TiO_2 NPs) has been done by sol-gel-hydrothermal colloidal route in two different apparatus; one being simple stainless steel (named as TiO_2-B) and other being at constant temperature and pressure autoclave (named as TiO_2-W). These TiO_2 NPs were investigated by various characterization techniques such as scanning electron microscope (SEM), X-ray diffractometer (XRD), and photoluminescence spectrophotometer. Also, it was observed that the quality of the synthesized TiO_2-W NPs is comparable with the commercial TiO_2 NPs (TiO_2-C), whereas the cost of synthesis is almost reduced to half. The synthesized TiO_2 NPs are used as the photoanode in dye-sensitized solar cell (DSSC). DSSC with TiO_2-W showed better power conversion efficiency as compared to DSSC with TiO_2-B.

GRAPHICAL ABSTRACT

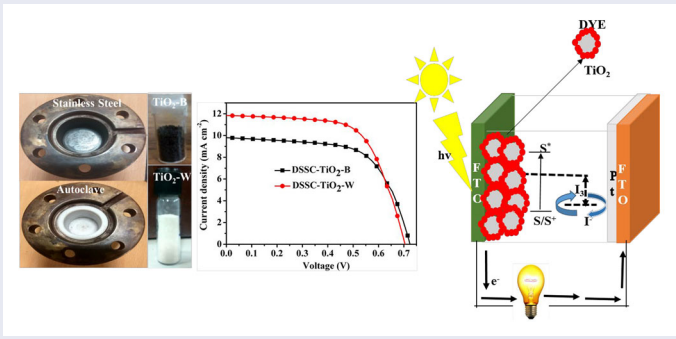

ARTICLE HISTORY
Received 29 August 2019
Accepted 24 November 2019

KEYWORDS
TiO_2; sol-gel; nanoparticles; dye-sensitized solar cells

Introduction

TiO_2 NPs have gained significant interest in the past owing to its various applications such as photocatalysis,[1] dye-sensitized solar cells (DSSCs),[2,3] water splitting, self-cleaning devices,[4] and many others. Among these applications, TiO_2 as photo-anode in DSSC used in enhancing the photo-conversion efficiency by converting the solar energy into electrical energy.[5] A DSSC is a low-cost solar cell based on a semiconductor formed between photoanode, electrolyte and a photosensitizer and formed a photoelectrochemical system. Here photoanode is used for charge transportation, the photoelectrons are provided from a separate photosensitizer. The charge separation occurs at the surfaces between the dye, semiconductor and electrolyte. Here, the free charge carriers are not generated by the excitation of band gap of TiO_2 rather they are generated by electron or hole injection of the excited dye. According to the general principle of DSSC, photo-voltage generated under illumination corresponds to the difference between the Fermi level of the electron in the solid and the redox potential of the electrolyte.[6] The sunlight passes through the transparent electrode (photoanode) into the dye layer where it can excite electrons that then flow into the titanium dioxide. The immersion of TiO_2 into the suitable electrolyte forms a depletion layer at the surface. The electric field in this depletion layer removes the injected elctron from the interface and stop their recombination with an oxidized dye. The N719 dye (sensitizer) is reproduced by redox electrolyte which receives electron back from the counter electrode.This is a regenerative cell that

CONTACT Shailesh Narain Sharma shailesh@nplindia.org CSIR-National Physical Laboratory, Dr K.S. Krishnan Road, New Delhi 110012, India; A. K. Hafiz ahafiz@jmi.ac.in Centre for Nanoscience and Nanotechnology, Jamia Millia Islamia, New Delhi 110025, India.
Color versions of one or more of the figures in the article can be found online at www.tandfonline.com/ldis.
Supplemental data for this article can be accessed on the publisher's website.

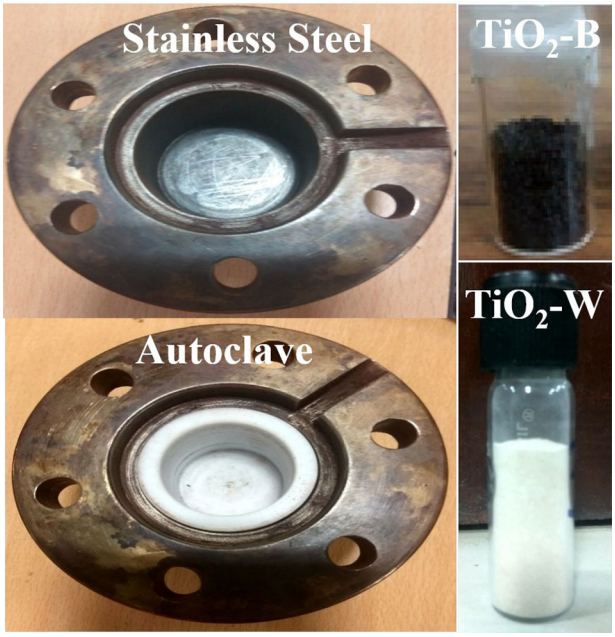

Figure 1. Different apparatus used for the synthesis of TiO_2 NPs.

upon absorbtion of sunlight, the effect is to drive electrons from the external circuit and convert light energy into electrical energy respectively. TiO_2[7] is used as a pigment in printing inks, plastics, cosmetics, soap, toothpaste and food.[8] It has many applications in dental implantation as well as the structure containing drugs.[9] TiO_2 mainly exists in three different forms: anatase, rutile, and brookite.[10] The anatase and rutile[11] have tetragonal while brookite has orthorhombic geometries respectively. The most stable form of TiO_2 is Rutile, and others are in the metastable. In general, the rutile form used for optical applications because of its high refractive index; pure brookite is also a fascinating candidate for photocatalytic[12] application. The nanocrystalline anatase form is used as a most suitable form in DSSC for photoanode[13,14] because it has lower surface energy and high surface area.[15] There are many methods of preparation of TiO_2[16] nanoparticles like low-pressure gas evaporation,[17] sputtering,[18] plasma,[19] high energy ball-milling,[20] and chemical depositions,[21] such as settling method, hydrolysis,[22] spraying,[23] oxidation-reduction, laser synthesis,[24] hydro-thermal, sol-gel, and electro-spark method.[25] Most commonly used methods are sol-gel, hydrolysis, hydro-thermal, co-precipitation, sluggish precipitation,[26] etc. The sol-gel method[27] is the cheapest method for preparation of nanoparticles, and it comprises of mixing, polymerizing, hydrolysis, ageing, and calcinations[28] of titanium precursor in aqueous solution.

Recently it has been reported, that in addition to as-synthesized white TiO_2, black TiO_2 obtained under hydrogenation treatment has gathered much attention in photovoltaics.[29] Here, black TiO_2 which is considered as a surface disordered material has been employed as photoanodes in DSSC.[30] In this report, TiO_2 nanoparticles synthesized by sol-gel technique followed by the low temperature annealing to obtain the anatase form of TiO_2 nanoparticles for photocatalytic[31] and DSSC application.[32] Here, two different types of TiO_2 such as TiO_2-W and TiO_2-B were synthesized in constant pressure hydrothermal autoclave and stainless steel chamber respectively. It is to be noted that here without using any hydrogenation treatment, we have obtained black TiO_2 with similar disordered structure as reported by others.[33,34] In this work, both as synthesized nanoparticles in autoclave and stainless steel abbreviated as TiO_2-W and TiO_2-B were utilized as a photo-anodes[35] in DSSC.[36] However, low efficiency obtained for dye-sensitized solar cells in TiO_2-B as compared to TiO_2-W can be attributed to the fact that in case of TiO_2-B, the number density of photogenerated charge carriers reduces, because of the presence of defects/impurities within the band gap which act as trapping centers and hence charge separation efficiency of TiO_2-B is less as compared to TiO_2-W.

The synthesis of TiO_2 nanoparticles at constant temperature and constant pressure autoclave conditions gives better efficiency as compared to the other process.

Experimental

The TiO_2 NPs were synthesized using sol-gel technique and were further annealed at 220 °C using two different apparatuses. The apparatus are shown in Figure 1 with the corresponding TiO_2 vials. The stainless steel apparatus without any Teflon lining results in black colored TiO_2 powder whereas the Teflon lined autoclave results in white colored TiO_2 powder. The TiO_2 nanoparticles synthesized in stainless steel and autoclave apparatus termed as TiO_2-B and, TiO_2-W, respectively and were compared with commercial TiO_2 nanoparticles named as TiO_2-C.Two types of photoanodes prepared by screen printing technique[35] used in dye-sensitized solar cells. The DSSCs contain photoanodes of TiO_2-B paste and TiO_2-W paste named as DSSC-TiO_2-B and DSSC-TiO_2-W, respectively. For experimental and characterization techniques information, please refer to Supporting Information.

Results and discussion

Crystallinity and phase

The XRD spectra for different TiO_2 NPs shown in Figure 2a. XRD spectra shows that both the synthesized NPs are highly crystalline, stable[37] and as per with the commercial NPs in terms of crystallinity. The synthesized NPs correspond to the anatase phase. The crystallite size is measured using Debye–Scherrer's formula:

$$\tau = \frac{K\lambda}{\beta \cos\theta} \quad [1]$$

where τ is the crystal size; λ is the wavelength of the X-ray radiation ($\lambda = 1.504$ Å) for Cu Kα; K took as 0.89 for spherical nanoparticles, and β is the line width at half-maximum height. The crystallite size with corresponding FWHM for all the three samples mentioned in Table 1.

Figure 2b shows the Raman spectra of TiO_2 nanoparticles of all the three samples. TiO_2-C shows five peaks at 141, 199, 396 (of minimal intensity), and 514 and 635 cm^{-1}. The Raman modes, at about 199 cm^{-1} is assigned to the mode of

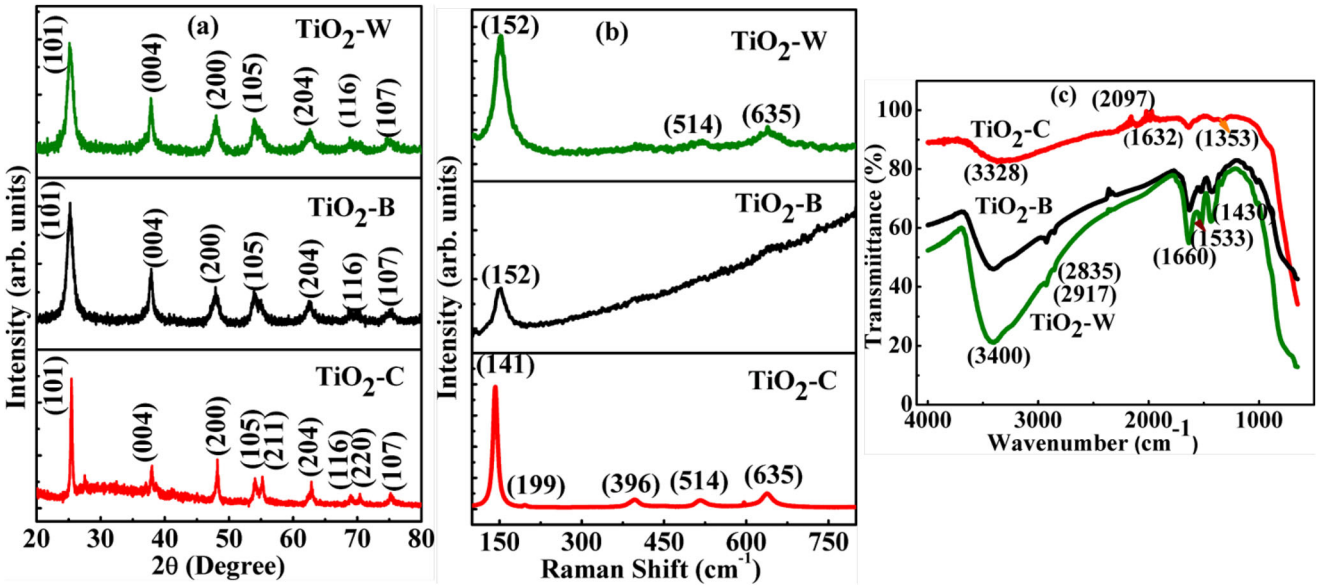

Figure 2. (a) XRD, (b) Raman, and (c) FTIR of TiO_2's NPs.

Table 1. FWHM and grain size of TiO_2 NPs as obtained from XRD spectra.

Materials	FWHM (β) (radian)	Grain size (τ) (nm)
TiO_2-W	0.0190	9.254
TiO_2-B	0.0194	8.645
TiO_2-C	0.0223	40.000

stretching, and the peak at 516 cm^{-1} is related to the bending and stretching vibration of Ti–O bonds while the band at 639 cm^{-1} is due to the Ti–O–Ti stretching vibration.[38] The TiO_2-W consists of three peaks (152, 514, 635) whereas TiO_2-B contains only one at 152 cm^{-1}, which is of minimal intensity. In TiO_2-W, peak at 635 cm^{-1} is of high intensity. Raman spectra showed that band shifting takes place toward the high-frequency side, and it reveals that with an increase in frequency, the particle size of TiO_2 nanoparticles decreases. The Raman spectra are the confirmation of the structure. The Raman analysis gives the agreement of TiO_2 anatase nanoparticles. The TiO_2-W is more conformational as compared to black TiO_2-B. Further, to identify the functional groups present on the surface of NPs, FTIR spectroscopy was done and shown in Figure 2c. The FTIR spectra showed several bands occurring at 3400, 2917, 2835, 1660, 1533, and 1430 in case of TiO_2-W and TiO_2-B as evident in Figure 2c, respectively. The FTIR spectra of TiO_2-C have characteristics bands at 3328, 2097, 1632, and, 1353 cm^{-1}. The absorption bands at 1533 and 3400 cm^{-1} are attributed to amine (–NH_2) and hydroxyl (–OH) stretching vibrations bands, respectively.[39] The stretching vibration is an indication of the presence of ligand acetic acid, which can control the size of TiO_2 nanoparticles. The bands are at 2917, 2835, 2097 cm^{-1} are due to stretching vibration of CH, CH2, CH3 functional groups. The IR band at 1600 cm^{-1} are due to C = C stretching vibrations. The bands are in the range of 1500–1400 cm^{-1} due to CH, CH2, CH3 bending vibrations and in range of 1400–1300 cm^{-1} which are due to C-OH alcohol group. The absorption spectra at 1405, 1430, 1530, and 2926 cm^{-1} were due to the banding of hydroxyl groups. The absorption band at 1632 cm^{-1} can be attributed to the amine or amide functional groups. The significant increase of bands centered at 2917 and 2835 cm^{-1} is due to the enhancement of TiO_2 concentration.

SEM and TEM analysis

The SEM images of all the three samples of TiO_2 nanoparticles shown in Figure 3a–3c. The SEM analysis reveals information about the surface morphology of TiO_2 nanoparticles showed that TiO_2 nanoparticles are agglomerated[40] polydisperse, spherical shape in nature.[41] In the case of TiO_2-W, the number density of the particles are more as compared to TiO_2-B, while TiO_2-C particles are more agglomerated and exactly spherical in nature.

The TEM images of all the three samples of TiO_2 shown in Figure 3d–3f which revealed that particles are spherical in shape with a narrow size distribution. From Figure 3d–3f, the agglomerated tetragonal crystallites with a particles size range of 7–15 nm can be observed with an average particle size found to be 7 nm which is in good agreement with the results obtained from XRD. The interplanar distances calculated from TEM are 0.31, 0.23, and 0.25 nm for TiO_2-W, B and, C, respectively. From the XRD analysis, it found that particles are highly crystalline with anatase phase, which is also confirmed by TEM lattice fringes.

Optical absorption analysis

The UV–visible spectra of TiO_2 nanoparticles shown in Figure 4a and compared with TiO_2-C. Figure 4b shows a UV–visible image of PEDOT: PSS. The absorbance band edge of TiO_2-W observed at 354, 360, for TiO_2-B at 400 nm for TiO_2-C and absorption edge for PEDOT: PSS found at 252 nm. Both the samples gave absorption in the UV–visible region. The results showed that the band gap energy and crystallites size are inversely proportional to each other, by the quantum confinement model.[42] The TiO_2-W has a

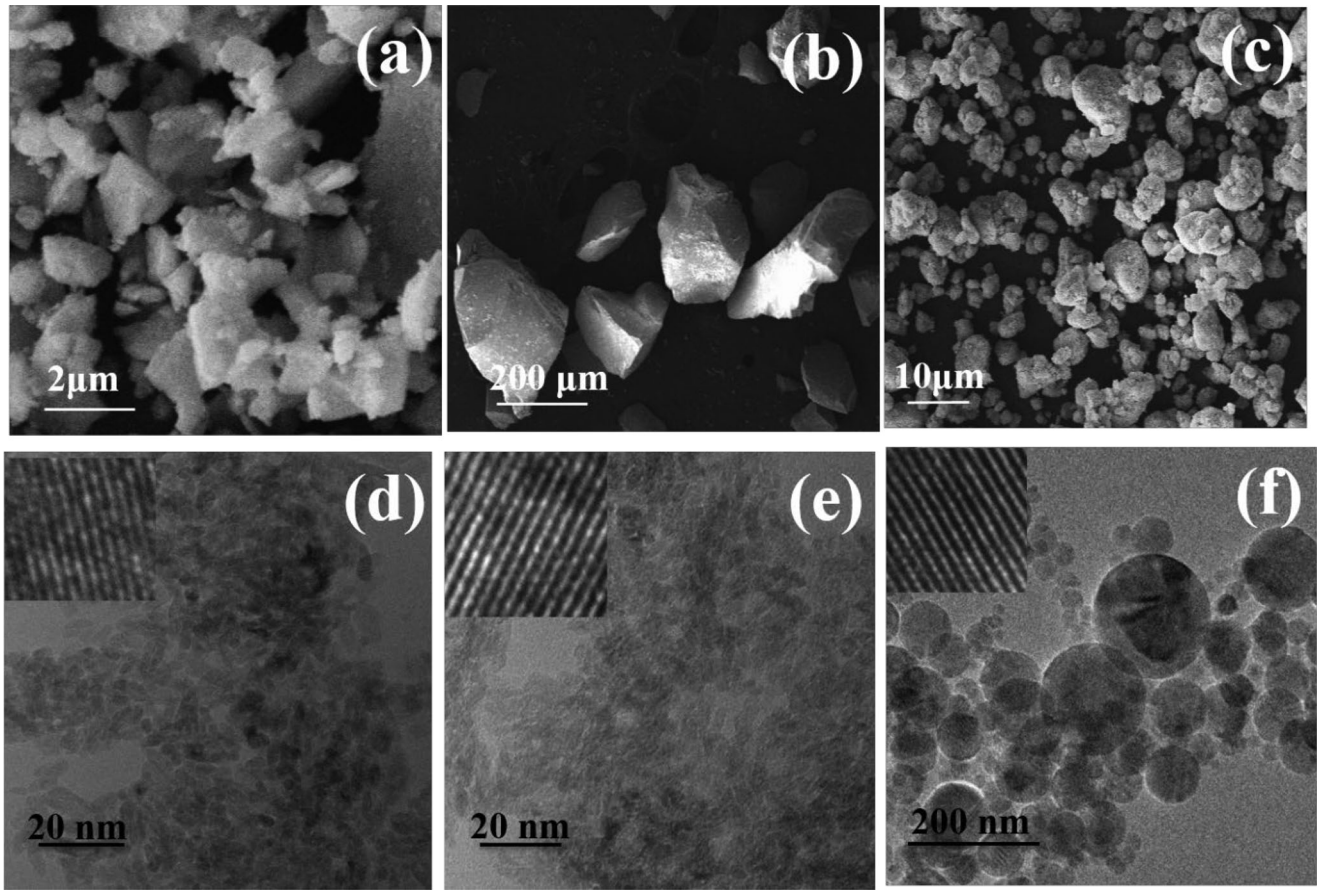

Figure 3. (a-c) SEM and (d-f) TEM of TiO_2's NPs.

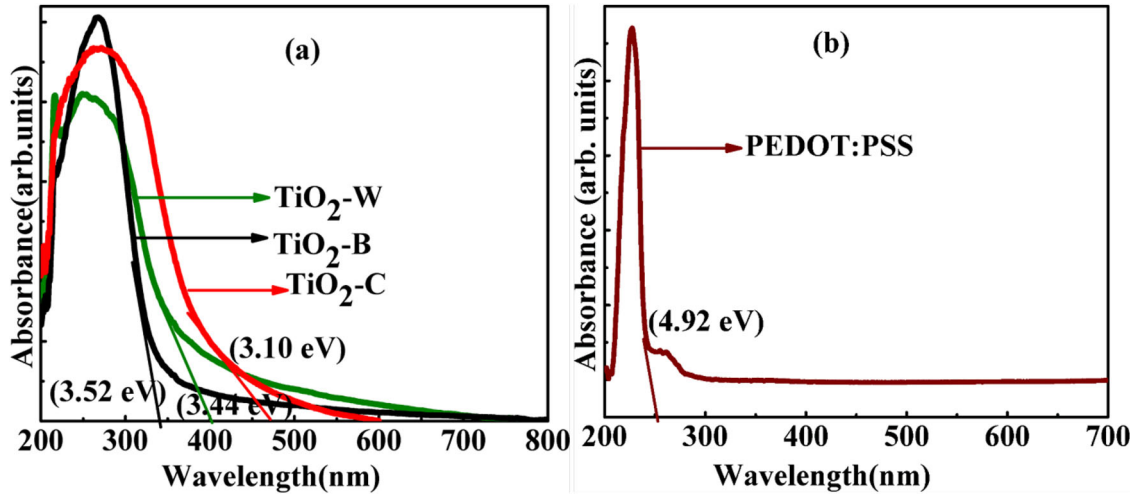

Figure 4. (a–c) UV–visible spectra of TiO_2's nanoparticles and (d) PEDOT: PSS, respectively.

Table 2. UV and PL parameters of different TiO_2's.

Materials	Excitation wavelength (nm)	Band gap (eV)	PL rate	K_{SV} (L^{-1})
TiO_2-W	360	3.44	0.703	5366.3
TiO_2-B	352	3.52	0.674	2789.8
TiO_2-C	400	3.10	0.722	6000.0
PEDOT:PSS	252	4.92	–	–

band gap of which is less than TiO_2-B, which means that TiO_2-W is more crystalline. The PEDOT: PSS has a band gap of 4.92 eV as we can see from Table 2. A quenching experiment carried out where PEDOT: PSS taken as donor and TiO_2 was chosen as a quencher as shown in Figure 5a. The Small aliquots of TiO_2 mixed with the PEDOT: PSS solution and the PL spectra recorded. The PL quenching[43] rate was calculated using the following formula.

$$\text{PL quenching rate} = \left(\frac{\text{PL}_{\text{initial}} - \text{PL}_{\text{final}}}{\text{PL}_{\text{initial}}}\right) \quad [2]$$

In the simplest case of PL quenching, the following relation is called the Stern–Volmer equation holds $\frac{I_0}{I} = 1 + K_{SV}$

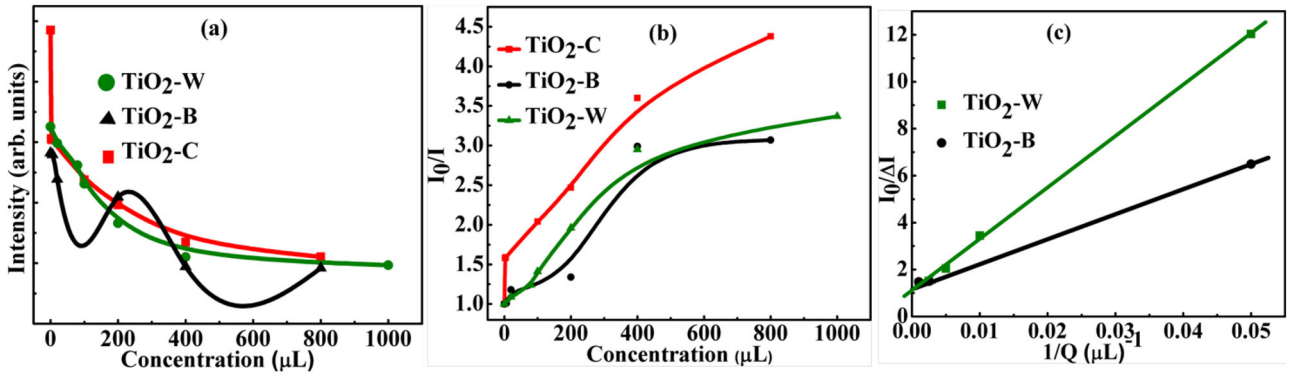

Figure 5. (a) PL Quenching from PEDOT: PSS to TiO_2's, (b) Stern–Volmer plot of TiO_2's between concentration and Intensity ratio, and (c) modified Stern–Volmer plot of TiO_2's between concentration and intensity ratio.

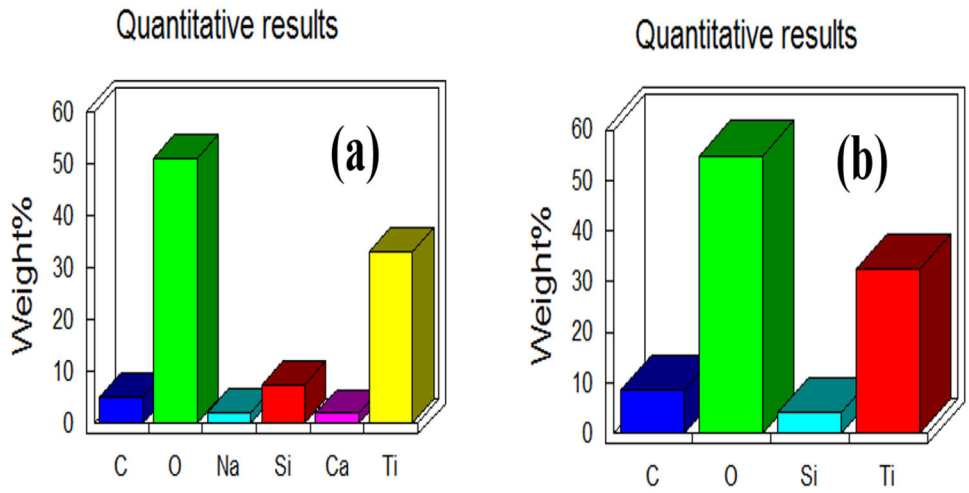

Figure 6. EDX of TiO_2's nanoparticles.

Table 3. Charge transfer parameter for different TiO_2's.

Materials	Accessible atoms (f_a)	Inaccessible atoms ($1 - f_a$)
TiO_2-W	0.907	0.092
TiO_2-B	0.818	0.181

where I_0 and I are the fluorescence intensities observed in the absence and presence of quencher, respectively. [Q] is the quencher concentration, and K_{SV} is the Stern–Volmer quenching constant.[44] A plot of I_0/I versus [Q] should yield a straight line with its slope equal to $K_{SV,}$ as shown in Figure 5b. From Table 2, we concluded that in the case of TiO_2-C, the charge transfer would be more as compared to TiO_2-W and B. But we also observed that TiO_2-W is the best quencher as compared to TiO_2-B. The steady-state PL Quenching described by Stern–Volmer plot, and coefficient of Stern–Volmer (Ksv) was obtained $K_{SV}=\left(\left[\frac{(I_0/I)}{Q}\right]\right)$.

From Table 2, we can see that the K_{SV} of TiO_2-W is almost similar to the TiO_2-C, whereas TiO_2-B has the least. The quenching phenomenon suggests that the TiO_2-W has excellent charge transfer properties and is comparable to the commercially available TiO_2. TiO_2-W has relatively more oxygen vacancy since annealed in vacuum conditions; whereas TiO_2-B has been annealed in stainless steel chamber in air ambient conditions and thus has less probability of oxygen vacancy and hence higher at.% and wt.% of O for TiO_2-B as compared to TiO_2-W as evident from EDX spectra (Figure 6) respectively. However, due to the presence of insufficient oxygen during the synthesis of TiO_2-B which creates defects and as a result, the charge carriers are trapped into the defects and are not available for the charge transfer which is also evident from Table 2. This effect is more in case of TiO_2-C as compared to TiO_2-W and TiO_2-B, respectively.

The modified Stern–Volmer plots for TiO_2-W and TiO_2-B for obtaining the no. of accessible and in-accessible atoms shown in Figure 5c. The accessible particles are those which are directly involved in the charge transfer, while Inaccessible particles are those who are not available for charge transfer.

$$f_a = \text{accessible atom and } 1 - f_a = \text{inaccessible atoms}$$

From Table 3, we found that in the case of TiO_2-W, the no. of inaccessible particles are less than as compared to TiO_2-B. However, TiO_2-W has more no. of accessible particles which are directly responsible for an enhanced charge transfer process. In case of TiO_2-W, band-to-band recombination of charge carrier is more since it is devoid of any defects, however in case of TiO_2-B which is not pure phase material[45] it is likely that there are certain defects/impurities which can act as traps with in the band gap which may leads to inferior charge recombination as compared to TiO_2-W. This may account for lower number of fluorophores for

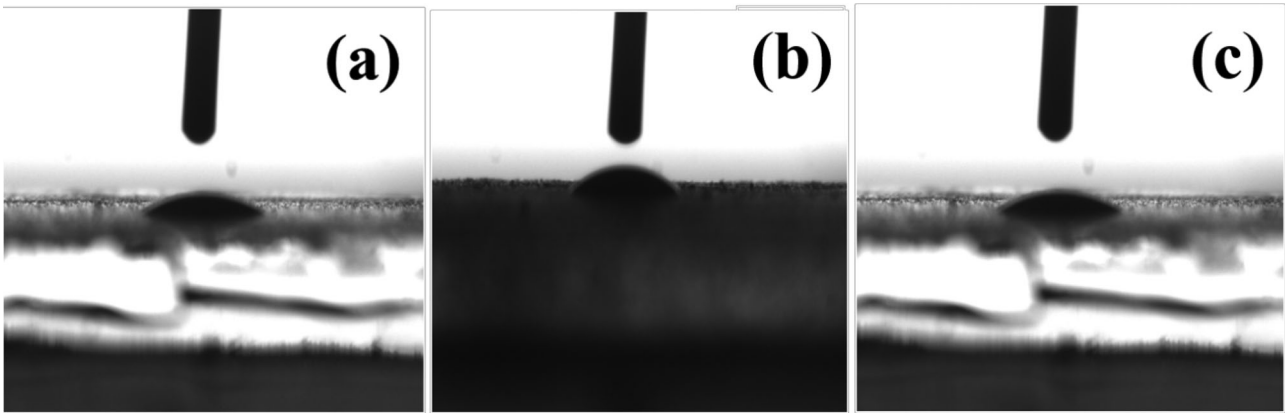

Figure 7. Contact angle of TiO_2's nanoparticles.

Table 4. Contact angle of TiO_2's.

Materials	Contact angle (°)
TiO_2-W	25°
TiO_2-B	35°
TiO_2-C	20°

accessible for TiO_2-B as compared to TiO_2-W. This is further clear from the EDX spectra (Figure 6), where the carbon impurities are more (higher at. and wt.%) and hence lower no. of fluorophores for TiO_2-B as compared to TiO_2-W for the PEDOT: PSS quencher can be understood.

The variation of PEDOT: PSS in composites is the same for both TiO_2-W and TiO_2-B before excitation, however upon excitation of these composites the number density of fluorophores differs in the composites leading to the difference in PL characteristics.

CA analysis

The contact angle (CA) measurements determine the wettability nature of the surface. If the contact angle is less than 90°, then wettability is low, and the surface is hydrophilic whereas if CA is more than 90°, then wettability is high and the surface is hydrophobic. The contact angle results shown in Figure 7a–7c demonstrates that TiO_2-W films exhibit less hydrophobicity (CA ~25°) as compared to corresponding films with TiO_2-B (CA ~35°) & TiO_2-C (CA ~20°), respectively shown in Table 4.

DLS analysis

The DLS is dynamic light scattering analysis, which is related to the Brownian motion of nanoparticles and measures the hydrodynamic diameter. The mean particle diameter (*Z*-average) for nanoparticles measured by DLS is always more massive than the particle size measured by TEM. Here, the *Z*-average value is 277.2 nm (0.474), 347.3 nm (0.68), and 831 nm (0.8) for TiO_2-W, TiO_2-B, and TiO_2-C, respectively where values in parenthesis represent polydispersity index (PDI) which is related with particle size distribution. Here, it found that the PDI value of TiO_2-W is the least as compared to the other two samples, which indicates the polydispersity of the former sample as compared

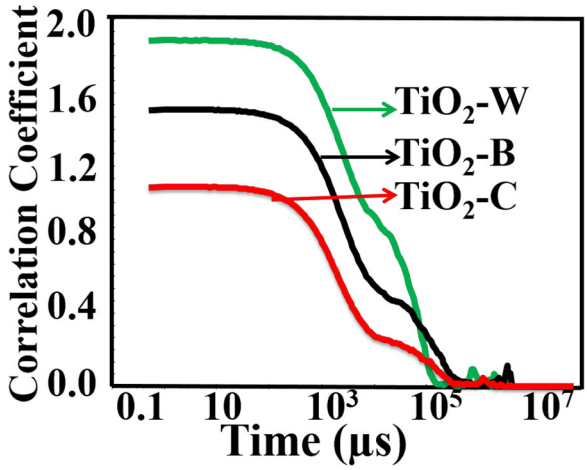

Figure 8. DLS measurement of TiO_2's nanoparticles.

to the latter samples. The *Z*-average analysis thus allows monitoring of NPs aggregation or release of NPs-surface modifiers. Figure 8 shows a plot of DLS correlation coefficient versus time for TiO_2-W, TiO_2-B, and TiO_2-C nanoparticles. From Figure 8, the correlation decay determines the sample polydispersity.

Photovoltaic performance

Figure 9 shows the *J–V* curve of DSSC-TiO_2-B and DSSC-TiO_2-W samples. DSSCs[46] parameters are given in Table 5. Here, DSSC-TiO_2-W shows better photovoltaic performance than the DSSC-TiO_2-B. The DSSC-TiO_2-W sample shows the short-circuit current density (JSC) of 11.83 mA cm^{-2}, open-circuit voltage (VOC) of 705 mV and overall PCE of 5.36%, while the DSSC-TiO_2-B sample exhibits the JSC of 9.80 mA cm^{-2}, VOC of 724 mV and PCE of 4.49%. Short circuit current density is large for TiO_2-W as compared to TiO_2-B, the favor of more dye adsorption and more efficient transportation.

The VOC[47] values of the DSSCs with the TiO_2-B is more than the TiO_2-W photoanode. The VOC is open circuit voltage which is related to the electronic Fermi level in the TiO_2 nanostructure and the redox potential of the electrolyte difference. During absorption phenomenon of dye N719, the proton transfer from the dye to TiO_2 surface,

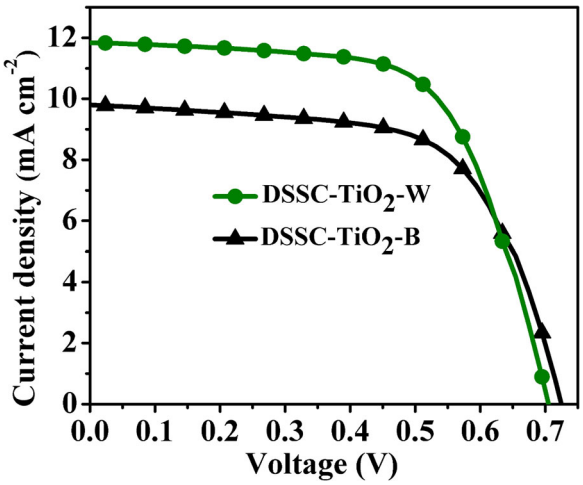

Figure 9. Photovoltaic performance of TiO_2's nanoparticles.

Table 5. Photovoltaic parameter of different TiO_2's.

Devices	J_{SC} (mA cm^{-2})	V_{OC} (mV)	FF (%)	PCE (%)
DSSC-TiO_2-B	9.80	724	63.36	4.49
DSSC-TiO_2-W	11.83	705	64.35	5.36

Fermi level of the electrons in TiO_2 has been positively shifted in TiO_2-W as compared to TiO_2-B, after that Fermi level shifts down due to positive charging. The modification in TiO_2 may ease the charge transfer from the N719 dye to the TiO_2 surface and the decrease in VOC. Moreover, the photo-stability of photovoltaic devices observed is a direct consequence of high crystallinity. Here, TiO_2-W sample is more crystalline as compared to TiO_2-B sample, which is directly related to the cell performance.

Conclusions

In this paper, TiO_2 nanoparticles synthesized by a sol-gel colloidal route using two different apparatus via an autoclave and stainless steel chamber has been found to have varied properties. For both TiO_2 (W/B), the NPs are crystalline, spherical in shape and polydisperse in nature as inferred from microscopic and DLS measurements. As elucidated from PL quenching and EDX measurements, in the case of TiO_2-W, band-to-band recombination of charge carriers and oxygen vacancies are more as compared to TiO_2-B. Here, TiO_2-W NPs has been annealed in vacuum conditions; whereas, TiO_2-B NPs has been annealed in stainless steel chamber in air ambience and thus has less probabilities of oxygen vacancy as compared to TiO_2-W. Moreover, in the case of TiO_2-B sample, the number density of photogenerated charge carriers and an effective charge separation reduces due to the presence of defects (carbon impurities as evident from EDX results which acts as traps as compared to TiO_2-W sample and hence the photovoltaic efficiency decreases for TiO_2-B. In addition, the autoclave method utilized in this work produces high quality of TiO_2 NPs, which are superior to both the stainless steel chamber synthesized TiO_2-B and commercial TiO_2-C NPs. Owing to the superior properties exhibited by TiO_2-W NPs, it exhibits better power conversion efficiency in DSSC as compared to TiO_2-B respectively.

Funding

Dr Sanjay Kumar Swami thanks to Department of Science and Technology, Ministry of Science and Technology, New Delhi, India for support through DST Inspire Faculty Award [DST/04/2015/002272]. Akanksha would like to thank CSIR for CSIR-GATE (SRF) fellowship.

References

[1] Ahmad, R.; Mondal, P. K. Adsorption and Photodegradation of Methylene Blue by Using PAni/TiO_2 Nanocomposite. *J. Dispers. Sci. Technol.* **2012**, *33*, 380–386. DOI: 10.1080/01932691.2011.567172.

[2] Swami, S. K.; Chaturvedi, N.; Kumar, A.; Dutta, V. Dye Sensitized Solar Cells Using the Electric Field Assisted Spray Deposited Kesterite (Cu_2ZnSnS_4) Films as the Counter Electrodes for Improved Performance. *Electrochim. Acta* **2018**, *263*, 26–33. DOI: 10.1016/j.electacta.2018.01.030.

[3] Swami, S. K.; Chaturvedi, N.; Kumar, A.; Dutta, V. Effect of Zinc Precursor on Cu_2ZnSnS_4 Nanoparticles Synthesized by the Solvothermal Method and Its Application in Dye-Sensitized Solar Cells as the Counter Electrode. *Mater. Today Energy* **2018**, *9*, 377–382. DOI: 10.1016/j.mtener.2018.06.008.

[4] Banerjee, S.; Pillai, S. C.; Falaras, P.; O'Shea, K. E.; Byrne, J. A.; Dionysiou, D. D. New Insights into the Mechanism of Visible Light Photocatalysis. *J. Phys. Chem. Lett.* **2014**, *5*, 2543–2554. DOI: 10.1021/jz501030x.

[5] Li, W.; Zeng, T. Preparation of TiO_2 Anatase Nanocrystals by $TiCl_4$ Hydrolysis with Additive H_2SO_4. *PLoS One* **2011**, *6*, e21082. DOI: 10.1371/journal.pone.0021082.

[6] Graetzel, M. Dye-Sensitized Solar Cells. *J. Photochem. Photobiol. C: Photochem. Rev.* **2003**, *4*, 145–153. DOI: 10.1016/S1389-5567(03)00026-1.

[7] Răileanu, M.; Crişan, M.; Drăgan, N.; Crişan, D.; Galtayries, A.; Brăileanu, A.; Ianculescu, A.; Teodorescu, V. S.; Nițoi, I.; Anastasescu, M.; et al. Sol–Gel Doped TiO_2 Nanomaterials: A Comparative Study. *J. Sol-Gel Sci. Technol.* **2009**, *51*, 315–329. DOI: 10.1007/s10971-009-2017-z.

[8] Maitani, M. M.; Tanaka, K.; Mochizuki, D.; Wada, Y. Enhancement of Photoexcited Charge Transfer by {001} Facet-Dominating TiO_2 Nanoparticles. *J. Phys. Chem. Lett.* **2011**, *2*, 2655–2659. DOI: 10.1021/jz2011622.

[9] Fujishima, A.; Honda, K. Electrochemical Photolysis of Water at a Semiconductor Electrode. *Nature* **1972**, *238*, 37–38. DOI: 10.1038/238037a0.

[10] Carp, O.; Huisman, C. L.; Reller, A. Photoinduced Reactivity of Titanium Dioxide. *Prog. Solid State Chem.* **2004**, *32*, 33–177. DOI: 10.1016/j.progsolidstchem.2004.08.001.

[11] Gupta, K. K.; Singh, N. L.; Pandey, A.; Shukla, S. K.; Upadayay, S. N.; Mishra, V.; Srivastava, P.; Lalla, N. P.; Mishra, P. K. Effect of Anatase/Rutile TiO_2 Phase Composition on Arsenic Adsorption. *J. Dispers. Sci. Technol.* **2013**, *34*, 1043–1052. DOI: 10.1080/01932691.2012.735937.

[12] Yu, J.; Yu, J. C.; Cheng, B.; Zhao, X. Photocatalytic Activity and Characterization of the Sol-Gel Derived Pb-Doped TiO_2 Thin Films. *J. Sol-Gel Sci. Technol.* **2002**, *24*, 39–48. DOI: 10.1023/A:1015109515825.

[13] Yoo, J. W.; Lee, S. M.; Kim, H. T.; El-Sayed, M. A. Shape Control of Platinum Nanoparticles by Using Different Capping Organic Materials. *Bull. Korean Chem. Soc.* **2004**, *25*, 395–396.

[14] Das, K.; Sharma, S. N.; Kumar, M.; De, S. K. Morphology Dependent Luminescence Properties of Co Doped TiO_2 Nanostructures. *J. Phys. Chem. C* **2009**, *113*, 14783–14792. DOI: 10.1021/jp9048956.

[15] León, A.; Reuquen, P.; Garín, C.; Segura, R.; Vargas, P.; Zapata, P.; Orihuela, P. FTIR and Raman Characterization of TiO_2 Nanoparticles Coated with Polyethylene Glycol as Carrier for 2-Methoxyestradiol. *Appl. Sci.* **2017**, *7*, 49. DOI: 10.3390/app7010049.

[16] Ishibai, Y.; Nishikawa, T.; Miyagishi, S. Synthesis of Nano-Sized TiO_2 Colloidal Sol and Its Optical Properties. *J. Dispers. Sci. Technol.* **2006**, *27*, 1093–1098. DOI: 10.1080/01932690600857147.

[17] Wang, X.; Wang, H.; Zhou, Y.; Liu, Y.; Li, B.; Zhou, X.; Shen, H. Confined-Space Synthesis of Single Crystal TiO_2 Nanowires in Atmospheric Vessel at Low Temperature: A Generalized Approach. *Sci. Rep.* **2015**, *5*, 8129. DOI: 10.1038/srep08129.

[18] Isai, M.; Ito, T.; Endo, T.; Sakai, T.; Hoshi, Y. Preparation of TiO_2 Thin Films by RF Magnetron Sputtering Method and Their Photocatalytic Properties. *Trans. Mater. Res. Soc. Jpn.* **2010**, *35*, 901–904. DOI: 10.14723/tmrsj.35.901.

[19] Macwan, D. P.; Balasubramanian, C.; Dave, P.; Chaturvedi, S. Thermal Plasma Synthesis of Nanotitania and Its Characterization. *J. Saudi Chem. Soc.* **2014**, *18*, 234–244.

[20] Indris, S.; Amade, R.; Heitjans, P.; Finger, M.; Haeger, A.; Hesse, D.; Grünert, W.; Börger, A.; Becker, K. D. Preparation by High-Energy Milling, Characterization, and Catalytic Properties of Nanocrystalline TiO_2. *J. Phys. Chem. B* **2005**, *109*, 23274–23278. DOI: 10.1021/jp054586t.

[21] Verhovšek, D.; Veronovski, N.; Lavrenčič Štangar, U.; Kete, M.; Žagar, K.; Čeh, M. The Synthesis of Anatase Nanoparticles and the Preparation of Photocatalytically Active Coatings Based on Wet Chemical Methods for Self-Cleaning Applications. *Int. J. Photoenergy* **2012**, *2012*, 10.

[22] Mahshid, S.; Askari, M.; Ghamsari, M. S. Synthesis of TiO_2 Nanoparticles by Hydrolysis and Peptization of Titanium Isopropoxide Solution. *J. Mater. Process. Technol.* **2007**, *189*, 296–300. DOI: 10.1016/j.jmatprotec.2007.01.040.

[23] Salim, N. T.; Yamada, M.; Nakano, H.; Fukumoto, M. The Synthesis of Titanium Dioxide (TiO_2) Powder for Cold Spray Process. *IOP Conf. Ser.: Mater. Sci. Eng.* **2011**, *18*, 032019. DOI: 10.1088/1757-899X/18/3/032019.

[24] Nath, A.; Laha, S. S.; Khare, A. Synthesis of TiO_2 Nanoparticles via Laser Ablation at Titanium-Water Interface. *Integr. Ferroelectr.* **2010**, *121*, 58–64. DOI: 10.1080/10584587.2010.492020.

[25] Sivalingam, G.; Nagaveni, K.; Hegde, M. S.; Madras, G. Photocatalytic Degradation of Various Dyes by Combustion Synthesized Nano Anatase TiO_2. *Appl. Catal. B-Environ.* **2003**, *45*, 23–38.

[26] Zanella, R.; Delannoy, L.; Louis, C. Mechanism of Deposition of Gold Precursors onto TiO_2 during the Preparation by Cation Adsorption and Deposition–Precipitation with NaOH and Urea. *Appl. Catal. A-Gen.* **2005**, *291*, 62–72.

[27] Oskam, G.; Poot, F. J. P. Synthesis of ZnO and TiO_2 Nanoparticles. *J. Sol-Gel Sci. Technol.* **2006**, *37*, 157–160. DOI: 10.1007/s10971-005-6620-3.

[28] Menon, N. G.; Tatiparti, S. S. V.; Mukherji, S. Effect of Calcination Temperature on the Microstructure and Electronic Properties of TiO_2–ZnO Nanocomposites and Implications on Photocatalytic Activity. *Appl. Nanosci.* **2018**, *8*, 915–930. DOI: 10.1007/s13204-018-0783-z.

[29] Zhang, K.; Park, J. H. Surface Localization of Defects in Black TiO_2: Enhancing Photoactivity or Reactivity. *J. Phys. Chem. Lett.* **2017**, *8*, 199–207. DOI: 10.1021/acs.jpclett.6b02289.

[30] Ullattil, S. G.; Thelappurath, A. V.; Tadka, S. N.; Kavil, J.; Vijayan, B. K.; Periyat, P. A Sol-Solvothermal Processed 'Black TiO_2' as Photoanode Material in Dye Sensitized Solar Cells. *Solar Energy* **2017**, *155*, 490–495. DOI: 10.1016/j.solener.2017.06.059.

[31] Barau, A.; Crisan, M.; Gartner, M.; Jitianu, A.; Zaharescu, M.; Ghita, A.; Danciu, V.; Cosoveanu, V.; Marian, I. O. Photothermal and Photocatalytic Processes on TiO_2 Based Materials Prepared by Sol-Gel Method. *J. Sol-Gel Sci. Technol.* **2006**, *37*, 175–178. DOI: 10.1007/s10971-005-6624-z.

[32] Li, Z.; Hou, B.; Xu, Y.; Wu, D.; Sun, Y.; Hu, W.; Deng, F. *Comparative Study of Sol–Gel–Hydrothermal and Sol–Gel Synthesis of Titania–Silica Composite Nanoparticles*; **2005**.

[33] Ni, W.; Li, M.; Cui, J.; Xing, Z.; Li, Z.; Wu, X.; Song, E.; Gong, M.; Zhou, W. 808nm Light Triggered Black TiO_2 Nanoparticles for Killing of Bladder Cancer Cells. *Materials Science and Engineering: C* **2017**, *81*, 252–260. DOI: 10.1016/j.msec.2017.08.020.

[34] Lü, X.; Chen, A.; Luo, Y.; Lu, P.; Dai, Y.; Enriquez, E.; Dowden, P.; Xu, H.; Kotula, P. G.; Azad, A. K.; et al. Conducting Interface in Oxide Homojunction: Understanding of Superior Properties in Black TiO_2. *Nano Lett.* **2016**, *16*, 5751–5755. DOI: 10.1021/acs.nanolett.6b02454.

[35] Beula, R. J.; Devadason, S.; Vidhya, B. Incorporation of Indium in TiO_2-Based Photoanodes for Enhancing the Photovoltaic Conversion Efficiency of Dye-Sensitized Solar Cells. *Appl. Nanosci.* **2018**, *8*, 1389–1397. DOI: 10.1007/s13204-018-0819-4.

[36] Ray, A. K.; Tracey, S. M.; Hodgson, S. Photoelectric Measurements on Chloroaluminium Phthalocyanine/Titanium Oxide Heterojunctions. *J. Sol-Gel Sci. Technol.* **2001**, *22*, 15–22. DOI: 10.1023/A:1011251917412.

[37] Mahlalela, L. C.; Ngila, J. C.; Dlamini, L. N. Characterization and Stability of TiO_2 Nanoparticles in Industrial Dye Stuff Effluent. *J. Dispers. Sci. Technol.* **2017**, *38*, 584–593. DOI: 10.1080/01932691.2016.1183501.

[38] Chellamuthu, J.; Girisun, T. C. S.; Vijaya, S.; Sambandam, A. Bacteriorhodopsin-Sensitized Preferentially Oriented One-Dimensional TiO2 Nanorod Polymorphs as Efficient Photoanodes for High-Performance Bio-Sensitized Solar Cells. *J. Photochem. Photobiol.* **2018**, *162*, 208–212.

[39] Sharma, S. N.; Vats, T.; Dhenadhayalan, N.; Ramamurthy, P.; Narula, A. K. Ligand-Dependent Transient Absorption Studies of Hybrid Polymer:CdSe Quantum Dot Composites. *Sol. Energy Mater. Sol. Cells* **2012**, *100*, 6–15. DOI: 10.1016/j.solmat.2011.10.020.

[40] Almusallam, A. S.; Abdulraheem, Y. M.; Shahat, M.; Korah, P. Aggregation Behavior of Titanium Dioxide Nanoparticles in Aqueous Environments. *J. Dispers. Sci. Technol.* **2012**, *33*, 728–738. DOI: 10.1080/01932691.2011.567886.

[41] Ullattil, S. G.; Narendranath, S. B.; Pillai, S. C.; Periyat, P. Black TiO_2 Nanomaterials: A Review of Recent Advances. *Chem. Eng. J.* **2018**, *343*, 708–736. DOI: 10.1016/j.cej.2018.01.069.

[42] Khalyavka, T.; Bondarenko, M.; Shcherban, N.; Petrik, I.; Melnyk, A. Effect of the C and S Additives on Structural, Optical, and Photocatalytic Properties of TiO_2. *Appl. Nanosci.* **2019**, *9*, 695–702. DOI: 10.1007/s13204-018-0838-1.

[43] Li, J.; Gong, Y.; Xu, J.; Wang, G.; Fang, G. Preparation and Nonlinear Optical Properties of Au Nanoparticles Doped TiO_2 Thin Films. *J. Sol-Gel Sci. Technol.* **2013**, *67*, 527–533. DOI: 10.1007/s10971-013-3110-x.

[44] Di Paola, A.; Bellardita, M.; Palmisano, L. Brookite, the Least Known TiO_2 Photocatalyst. *Catalysts* **2013**, *3*, 36–73. DOI: 10.3390/catal3010036.

[45] Tian, M.; Mahjouri-Samani, M.; Eres, G.; Sachan, R.; Yoon, M.; Chisholm, M. F.; Wang, K.; Puretzky, A. A.; Rouleau, C. M.; Geohegan, D. B.; et al. Structure and Formation Mechanism of Black TiO_2 Nanoparticles. *ACS Nano* **2015**, *9*, 10482–10488. DOI: 10.1021/acsnano.5b04712.

[46] Shahid, M. U.; Mohamed, N. M.; Muhsan, A. S.; Khatani, M.; Bashiri, R.; Zaine, S. N. A.; Shamsudin, A. E. Dual Functional Passivating Layer of Graphene/TiO_2 for Improved Performance of Dye-Sensitized Solar Cells. *Appl. Nanosci.* **2018**, *8*, 1001–1013. DOI: 10.1007/s13204-018-0685-0.

[47] Ito, S.; Murakami, T. N.; Comte, P.; Liska, P.; Grätzel, C.; Nazeeruddin, M. K.; Grätzel, M. Fabrication of Thin Film Dye Sensitized Solar Cells with Solar to Electric Power Conversion Efficiency over 10%. *Thin Solid Films* **2008**, *516*, 4613–4619. DOI: 10.1016/j.tsf.2007.05.090.